Seismic noise-based methods for soft-rock landslide characterization

OMBELINE MÉRIC[1,2], STÉPHANE GARAMBOIS[1,4], JEAN-PHILIPPE MALET[3], HÉLOÏSE CADET[4,5], PHILIPPE GUÉGUEN[4] and DENIS JONGMANS[1,4]

Key words. – Seismic noise, Soft-rock landslide, *In-situ* characterization, 3D geometry

Abstract. – In order to better understand the mechanics and dynamic of landslides, it is of primary interest to image correctly their internal structure and their slip surface. Several active geophysical methods are able to provide the geometry of a given landslide, but were rarely applied in 3 dimensions in the past. The main disadvantages of methods like seismic reflection and electrical tomography are that there are heavy to set up and/or to process, and they consequently are expensive and time consuming. Moreover, in the particular case of soft-rock landslides, their respective sensitivity and resolution are not always adequate to locate the potential slip surfaces. Passive methods may represent an interesting alternative particularly for landslides difficult to access, as they require lighter instrumentation and easier processing tools. Among them, the seismic noise based methods have shown increasing applications and developments, in particular for seismic hazard mapping in urban environment. In this paper, we present seismic noise investigations carried out on two different sites, the "Super Sauze" mudslide and the "Saint Guillaume" translational clayey landslide (France), where independent measurements (geotechnical and geophysical tests) were performed earlier. Our investigations were composed of electrical tomography profiles, seismic profiles for surface-wave inversions, H/V measurements, which are fast and easy to perform in the field, in order to image shear wave contrasts (slip surfaces), and seismic noise array method, which is heavier to apply and interpret, but provides (S)-waves velocity profile versus depth. For both sites, landslide bodies are characterized by lower S wave velocity (Vs < 300 m.s⁻¹) and lower resistivity (ρ < 60 Ohm.m) than in the stable part (Vs > 550 m.s⁻¹; ρ > 150 ohm.m). Their thickness vary from a few m to 50 m. Comparison between geophysical investigations and geotechnical data proved the applicability of such passive methods in 3D complex structures, with however some limitations.

Caractérisation de glissements de terrain argileux par des méthodes de bruit de fond sismique

Mots clés. – Bruit de fond sismique, Glissement de terrain argileux, Caractérisation *in-situ*, Géométrie 3D

Résumé. – Afin d'identifier les mécanismes de contrôle et de caractériser la dynamique de glissements de terrain, il est impératif d'imager correctement leur structure interne et leur surface de glissement. Plusieurs méthodes de prospection géophysique de proche surface sont utilisables pour identifier la géométrie d'un glissement de terrain, mais leurs potentialités ont été rarement testées en 3D. Les principaux inconvénients de méthodes géophysiques telles que la sismique réflexion ou la tomographie électrique sont la difficulté de mise en œuvre et/ou la complexité des traitements de données, ce qui les rend chères et consommatrices en temps. De plus, pour le cas particulier de glissements argileux, leur sensibilité et résolution ne sont pas toujours adaptées à la détection des surfaces de glissement. Les méthodes géophysiques passives, qui offrent l'avantage d'une instrumentation légère et d'un traitement des données plus simple, représentent ainsi une alternative intéressante, particulièrement pour les mouvements de terrain difficiles d'accès. Parmi celles-ci, les méthodes de bruit sismique ambiant connaissent depuis quelques années des développements et applications intéressants, notamment pour le zonage de l'aléa sismique en milieu urbain. Nous présentons dans ce papier des investigations par bruit de fond sismique effectuées sur deux sites instables, le glissement-coulée de "Super Sauze" et le glissement translationnel de "Saint Guillaume" (France), où des investigations géotechniques et géophysiques indépendantes étaient disponibles.

Nos investigations se composent (1) de tomographies électriques, de profils sismiques pour l'analyse des ondes de surface et de mesures H/V, simples, légères et rapides à installer sur site, afin de cartographier des contrastes de vitesse d'onde S (surface de glissement) et (2) de mesures de bruit de fond réseau, plus délicates et complexes à déployer sur site et à interpréter, mais qui permettent d'accéder à des profils de vitesses d'ondes S en fonction de la profondeur. Les deux glissements sont caractérisés par de plus faibles vitesses d'onde de cisaillement (Vs < 300 m.s⁻¹) et de plus faibles résistivités (ρ < 60 ohm.m) dans le corps du glissement que dans la partie stable (Vs > 550 m.s⁻¹; ρ > 150 ohm.m). Leurs épaisseurs varient de quelques mètres à 50 m. Les comparaisons entre nos investigations géophysiques et les sondages géotechniques prouvent l'applicabilité des méthodes géophysiques passives dans des environnements 3D, mais indiquent également certaines limites.

1. 'Laboratoire Interdisciplinaire de Recherche Impliquant la Géologie et la Mécanique' (LIRIGM), EA 3111 UJF, Maison des Géosciences, BP 53, F-38041 Grenoble cedex 9, France. Tel. +33 (0)476 828 046 / Fax. +33 (0)476 828 070 / E-mail : ombeline.meric@ujf-grenoble.fr
2. 'Société Alpine de Géotechnique' (SAGE), ZI de Mayencin, BP 17, F-38610 Gières, France.
3. 'Faculty of Geosciences', UCEL, Utrecht University, Po Box 80.115, NL-3508 TC Utrecht, Netherlands.
4. 'Laboratoire de Géophysique Interne et Tectonophysique' (LGIT), UMR 5559 CNRS-UJF-US, Maison des Géosciences, BP 53, F-38041 Grenoble cedex 9, France.
5. 'Centre d'Etude Technique de l'Equipement' (CETE), Antenne Méditerranée, Laboratoire Régional de Nice, 56 Boulevard Stalingrad, F-06359 Nice cedex 4, France.

INTRODUCTION: STATE OF THE ART AND SCIENTIFIC ISSUES

Authorities responsible for protecting human lives as well as infrastructures from the threat of landslide hazard are particularly concerned with three critical aspects: (1) the spatial distribution of the processes, (2) the understanding of their mechanisms, (3) their magnitude and temporal frequency. These concerns imply accurately assessing landslide characteristics and evaluating their controlling factors (climate or seismic triggers) in a dynamic dimension. For these reasons, 2D and 3D mathematical models have been developed during the last decade in order to simulate the complexity of landslide mechanisms [Commend *et al.*, 2004; Malet *et al.*, 2005; Tacher *et al.*, 2005]. Presently, one of their main weaknesses lies in the large uncertainty of parameters describing the unstable area. For example, critical information such as the 3D geometry of a landslide, its geomechanical and hydrological properties, or its internal discontinuities, as well as the uncertainties associated to these parameters, are rarely available.

Landslides are generally studied using geotechnical investigations (boreholes, penetrometric tests, etc), local instrumentation placed in boreholes (piezometers, inclinometers), as well as detailed geomorphological observations [Giraud *et al.*, 1991; Flageollet *et al.*, 2004]. Even though these studies provide direct information on the landslide material, their cost and limited spatial representativeness hinder their use for 3D studies. In particular, except by multiplying the number of tests, these methods are not able to image the lateral variability of landslide characteristics. To address this problem, a large selection of geophysical methods is available on a broad spatial scale. An increasing trend to apply geophysical studies for landslide characterization has been recently observed, mainly thanks to the improvement of data-acquisition systems and of data-inversion softwares. A critical review of these methods is discussed by Jongmans and Garambois [2007], who point out the need of combining geophysical methods [Israil and Pachauri, 2003] and of validating geophysical data with geotechnical information [Maquaire *et al.*, 2001; Flageollet *et al.*, 2004]. In practice, 3D geophysical investigations of large active landslides can be time consuming and expensive. Consequently, fast and low costs methods, with instruments easy to deploy have to be developed in the future, at least to locate the slip surfaces and to characterize bedrock geometries in 3D. Methods based on seismic noise measurements, which were extensively applied for seismic hazard mapping in the recent years [Asten, 2004], fill part of those criteria.

In this paper, we present two examples of seismic noise investigations carried out on two soft-rock landslides of the South French Alps (fig. 1), *e.g.* the "Super-Sauze" mudslide in the black marls of the Ubaye valley and the "Saint-Guillaume" translational landslide in the varved clays of the Trièves Plateau. At both sites, the slip surfaces are located within a homogeneous clay formation. The purposes of our studies are to evaluate the potential of seismic noise data, first to detect the slip surfaces using the H/V spectral ratio and second, to derive (S)-wave velocity profiles using networks. Very few seismic noise investigations were performed on landslides so far. Gallipoli *et al.* [2000] briefly mentioned the use of H/V methods on the large "Giarossa" landslide (southern Italy), which helped to interpret electrical tomography images.

Recently, Méric *et al.* [2005] failed to identify the slip surface of the "Séchilienne" large rocky landslide using H/V measurements. They however noted a clear correlation between amplitude of the seismic noise and the landslide displacement rate explained by fracture density. As both "Super-Sauze" and "Saint-Guillaume" landslides were characterized and monitored using geotechnical and geophysical measurements, a critical discussion of the results provided by seismic noise methods is possible.

SEISMIC NOISE THEORY

The H/V method involves computing the spectral ratio between the horizontal and vertical components of the seismic noise recorded simultaneously at a given location with a 3D seismometer placed at the ground surface. Nogoshi and Igarashi [1971] first proposed the use of the H/V method as a tool for the estimate of the seismic response of the surface layers. This method has since been widely diffused around the world by Nakamura [1989]. Since 1989, because of its low-cost and its fast deployment, H/V method has become widespread used, mainly with the objective of detecting the sedimentary zones that could amplify seismic ground
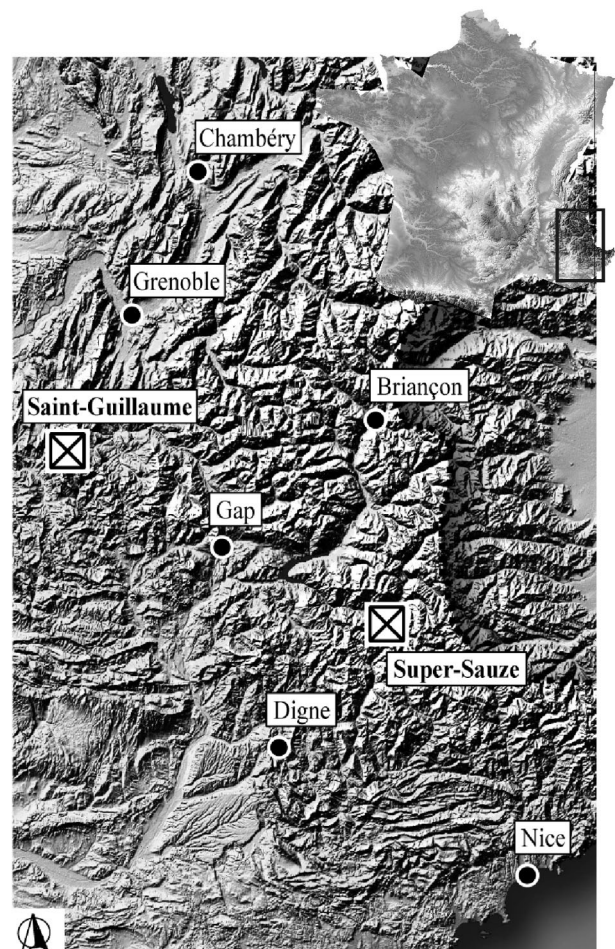

FIG. 1. – Location of the two test sites in the South French Alps: mudslide of "Super-Sauze" and translational landslide of "Saint-Guillaume".

FIG. 1. – *Localisation des deux sites tests dans les Alpes du Sud de la France : glissement-coulée de "Super-Sauze" et glissement translationel de "Saint-Guillaume".*

motion. The validation of the H/V method has been since confirmed both experimentally [Lermo and Chávez-García, 1993; Field and Jacob, 1995; Guéguen *et al.*, 2000; Lebrun *et al.*, 2001] and from theoretical and numerical studies [Field and Jacob, 1993; Lachet and Bard, 1994; Cornou *et al.*, 2004; Bonnefoy-Claudet, 2004]. In the case of a stratified soil profile composed of a soft layer on top of a stiffe bedrock, the amplified frequency f_0 may be estimated using the equation $f_0=Vs/4Hs$ [Haskell, 1960], where Hs is the thickness and Vs the shear wave velocity of the topmost layer, respectively, provided that the (S)-wave contrast is sufficiently large [Bonnefoy-Claudet, 2004]. As outlined by the equation linking f_0 to Hs, knowing the shear wave velocity Vs of the upper layer is fundamental to deduce the thickness of this layer. This information can be derived from (S)-wave refraction or surface wave analyses. Nevertheless, the simple relation linking fundamental frequency, shear wave velocity and depth is valid for a 1D model, which is not the geometry of most valleys. For instance, Steimen *et al.* [2003] and Roten *et al.* [2004] recently showed experimentally the strong 2D effect of valley shape on the resonance frequency deduced from ambient seismic noise. However, according to the concept of critical shape ratio proposed by Bard and Bouchon [1985], who numerically studied the dynamic response of various 2D structures shapes, the seismic behaviour of both landslides should be mainly characterized by one-dimensional resonance and surface wave propagation. A shear-wave velocity depth-profile can also be obtained from seismic noise measurements recorded by an array of seismometers, which allow the dispersion curve of Rayleigh-wave phase velocity to be computed [Tokimatsu, 1997; Satoh *et al.*, 2001; Scherbaum *et al.*, 2003].

In the following, all dispersion curves deduced from active surface-wave (e.g surface waves recorded during seismic refraction acquisitions) or from seismic noise network analyses, were computed using the conventional semblance-based frequency-wavenumber method [Lacoss *et al.*, 1969; Kvaerna and Ringdahl, 1986; Ohrnberger, 2001], which provides a semblance map of the velocity (or slowness) and frequency of the waves travelling with the highest energy. The obtained dispersions curves have been inverted to obtain a (S)-wave vertical velocity depth-profile. We used a neighbourhood algorithm inversion method for which computation time was optimized [Wathelet *et al.*, 2004]. This method is a stochastic direct search method for finding models of acceptable data fit within a multidimensional parameter space [Sambridge, 1999a; 1999b]. Four parameters were investigated, *i.e.* thickness, density, (P)-wave velocities and (above all) (S)-wave velocities of each layer. Thousands of direct models were tested and only those exhibiting lower RMS errors were kept. To reduce the number of good fitting models, the H/V resonance frequency of the central station was added as a additional constrain during the inversion process.

INVESTIGATION OF THE "SUPER-SAUZE" MUDSLIDE

Geological, geomorphological and geotechnical setting of the mudslide

The "Super-Sauze" mudslide (Ubaye valley) is one of the persistently active slides (since the 1970's) occurring in black marls [Malet and Maquaire, 2003]. Its geological environment is very complex and is the consequence of the geological history of this alpine zone characterized by an overthrust of allochtonous sandstone and limestone formations over the autochthonous black marl bedrock. From the highest to the lowest elevations, geology consists of: (1) the calcareous Klippe of Lan which overhangs the mudslide, (2) a moraine deposited by the Ubaye glacier during the Quaternary, (3) a bedrock consisting of Callovo-Oxfordian black marls with a grey clayey schist facies, very finely laminated and highly tectonized.

The "Super-Sauze" mudslide is a clayey flow-like landslide characterized by a complex vertical structure associating a slip surface and a viscoplastic plug. Multidisciplinary observations (geology, geomorphology, geotechnics, hydrology) carried out since 1991 [Weber and Hermann, 2000; Flageollet *et al.*, 2004] provide substancial information about its geology and geometry. The mudslide material consists of a silty-sand matrix mixed with moraine debris. It extends over an horizontal distance of 850 m and occurs between an elevation of 2105 m at the crown and 1740 m at the toe with an average 25° slope. Its total volume is estimated at 750,000 m³ and creeping velocities range from 0.01 to 0.4 m.day⁻¹ [Malet and Maquaire, 2003]. A detailed morphological description of the mudslide since its genesis can be found in Weber and Herrmann [2000]. The bedrock topography corresponds in the upper part to a succession of more or less parallel crests and gullies and, in the medium and lower parts, to a narrow and deeply incised channel. Consequently, its thickness is highly variable and varies between 0 and approximately 20 m. This geometrical scheme plays an essential role in the dynamics of the landslide by delimiting preferential water and material pathways and creating sections with differing kinematical, mechanical and hydrological characteristics. Its geotechnical structure consists in two superimposed units [Flageollet *et al.*, 2004; Malet and Maquaire, 2003]. The topmost unit, 5 to 9 m thick, is a very wet muddy formation, whereas the lowermost unit, with a maximum thickness of 10 m, is a stiff compact, relatively impervious and apparently stable formation. The hillslopes delimitating the lateral extension of the mudslide are characterized by moraine deposits, 3 to 15 m thick, especially on the eastern flank.

Electrical tomography

Six electrical tomography profiles were carried out on the mudslide allowing a pseudo-3D view of its internal structure (fig. 2, white lines). The tomography profiles were acquired using a Wenner configuration selected for its high signal to noise ratio property and its sensitivity to horizontal contrasts. This configuration is less adapted to accurately image lateral contrasts [Dahlin and Zhou, 2004]. Three transverse profiles A1, A2 and A3 were acquired using 64 electrodes spaced at 4 m in the upper part of the mudslide. Two transverse profiles C1 (80 electrodes, 4 m spacing) and C2 (48 electrodes, 5 m spacing) were acquired in the middle part of the mudslide. Finally, longitudinal profile CA (64 electrodes, 5 m spacing) was performed between transects C1 and A1. The raw data were inverted independently in 2D using the RES2DINV inversion software [Loke and Barker, 1996], considering a L2-norm for optimisation. The
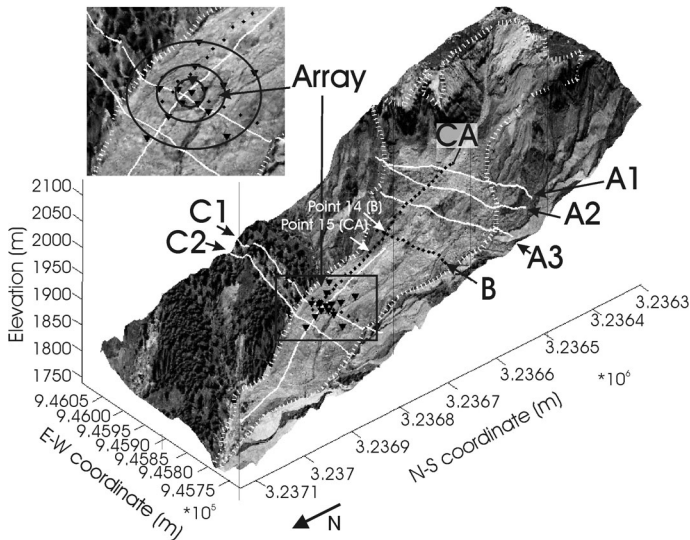
FIG. 2. – 3D topography image of the "Super-Sauze" mudslide and locations of the geophysical measurements. White lines: electrical tomography profiles; black dots: seismic noise measurements (H/V); black triangles: seismic noise network.
FIG. 2. – *Image 3D de la topographie du glissement-coulée de "Super-Sauze" et positionnement des mesures géophysiques et de bruit de fond sismique. Lignes blanches : tomographies électriques ; points noirs : points de mesures du bruit de fond sismique (H/V) ; triangles noirs : capteurs du bruit de fond réseau.*

derived resistivity sections have RMS errors lower than 3% after 5 iterations.

The electrical sections (fig. 3) show a contrast between the mudslide material with low resistivity values (lower than 60 ± 24 Ω.m) and the stable bedrock with higher resistivity values (higher than 150 ± 60 Ω.m). These resistivity values are comparable with those obtained by Schmutz *et al.* [2000] from joint-inversion of VES and TDEM data, who found resistivities ranging from 2 to 50 Ω.m for the active unit and more than 400 Ω.m for the bedrock. The increase of resistivity values with depth observed in the mudslide material can be explained by a decrease of the hydraulic conductivity with depth due to both the presence of water-saturated cracks in the topmost layer and compaction of the lowermost layer. On the eastern part of profiles C1 and C2, higher resistivity values (more than 700 Ω.m) are observed; they correspond to stable hillslopes made of moraine deposits. Bellow the eastern part of the landslide body on profile C1, a high resistivity anomaly is imaged, which probably corresponds to a former coarse landslide mainly composed by moraine deposits. These results agree with geotechnical investigations, which outline the transverse and the longitudinal thickness changes of the mudslide, underlying its complex bedrock topography.

In the middle part of the mudslide, the electrical sections indicate a total thickness ranging from 24 m to less than 5 m along profiles C1 and C2; this geometry is consistent with the depth variations proposed by Malet and Maquaire [2003] for this section on the basis of geotechnical tests. In the upper part of the mudslide, a more or less constant thickness of 18 m is found along profile A1, while profiles A2 and A3 indicate strong lateral changes due to the presence of bedrock crests. These profiles point out a deeper bedrock (more than 30 m) than in the middle part.

Although geotechnical data are more scarce in this part of the mudslide, the resistivity variations agree with the combined geomorphological-geotechnical interpretation suggested by Malet [2003]. The surface formations show larger resistivity values probably due to dryer hydrological conditions in autumn. Finally, the longitudinal electrical image indicates smooth vertical variations of the mudslide thickness, with a maximum value of 18 m at the intersection with profile C1.

These electrical data will be used in zones lacking of geotechnical measurements for interpreting the seismic noise measurements, assuming that the slip surface is localized at the 60-150 ohm.m contrast.

H/V method

Three H/V seismic noise profiles were performed on the mudslide (fig. 2). Two of them (C and B) were carried out in the transverse direction along geotechnical cross-sections, with a seismometer spacing of respectively 15 m and 10 m. A longitudinal profile (CA) was acquired between geotechnical cross-sections A and C with a 10 m spacing. The experimental device included six 3D Lennartz sensors (5 seconds), which have a flat response in the [0.2-50 Hz] frequency range, connected to a CityShark[TM] II acquisition system developed for seismic noise measurements [Chatelain *et al.*, 2000]. Ambient vibration data were sampled at 200 Hz and recorded for 30 minutes (fig. 4a). From this dataset, as many as possible short time-windows (about 40 seconds in duration) were selected using an anti-trigger process in order to select signals presenting the most uniform noise ratio, *i.e.* without transient high-frequency waves (grey selections on figure 4a). The procedure to detect transients is based on a comparison between the short term average "STA", e.g., the average level of signal amplitude over a short period of time (1 s) and the long term average "LTA", e.g., the average level of signal amplitude over a much longer period of time (30 seconds). For this application the STA/LTA ratio must remain below a small threshold value (typically around 1.5-2) over a sufficient duration. Finally each of the three components time signals were fast Fourier transformed and the spectral ratio was computed for each horizontal component (*e.g.*, H_1/V and H_2/V) as well as for the root mean square of the spectral ratio (H/V). To investigate complex and irregular structures, Uebayashi [2003] suggested orientating one component of the seismometer parallel to the main structure as the frequency peak amplitude is sensitive to the orientation of the horizontal component. Figures 4b and 4c show spectral ratio computed using the E-W component, the N-S component and the H component (square root of E-W and N-S components) for point 15 of profile CA and for point 14 of profile B respectively (fig. 2). Both points are located in the area where 2D effects were detected on the H/V data. Figure 4b shows a similar frequency peak around 11 Hz obtained from both E/V and N/V ratios. However, the amplitude of these peaks range from 1.8 for the N/V ratio to 2.8 for the E/V ratio. On contrary, figure 4c exhibits different frequency peaks (9 Hz on N/V ratio, 11 Hz on E/V ratio) with similar amplitudes. These variations of spectral ratio amplitude (fig. 4b) and of the value of the amplified frequency f_0 are probably caused by 2D or 3D effects. In order to take this effect into account, the spectral ratio was computed using the E-W

component on profiles CA and C, as the most important structure change is expected to occur along the longitudinal axis of the mudslide. On profile B, the spectral ratio was computed using the N-S components because the geotechnical investigations indicate large lateral variations in the bedrock depth.

Figures 5a, 5b and 5c present H/V spectral ratios calculated in the [0.2-20 Hz] frequency range for the profiles B, C1 and CA as a function of frequency and location along each profile. Colours represent the neperian logarithm of the horizontal to vertical spectral ratio. The black dotted points show the picked frequency peaks and the white dot lines locate the intersections with other profiles. Figure 5d maps the spatial variation of the picked frequency (colour scale) including those acquired during the seismic noise network experiment.

On profile CA, a clearly distinguishable dominant frequency can be easily picked on most point measurements; this dominant frequency varies smoothly from 4 to 11 Hz along the profile. For some points, higher frequencies exhibiting stronger H/V amplitudes could have been wrongly picked (*eg.*, like for point 7, with two major frequencies around 10 Hz and 15 Hz) but also lower frequencies at some other points. Even if the landslide structure is 3D, the dominant frequency varies continuously, resulting from the smooth variations of the thickness along the profile and by a well-adapted spatial sampling (10 m). In this case, no 3D effect significantly disturbed data acquisition and data processing, implying that surface wave propagation can be considered as 1D [Bonnefoy-Claudet, 2004]. On profile B several resonance frequencies can be picked at single point measurements, probably generated by interferences from several layers. A blind frequency picking carried out by looking for the maximum of H/V amplitudes resulted in too strong heterogeneities. Consequently, we decided to pick two frequencies at some points, where we propose a non-unique interpretation (fig. 6), considering the presence

of several layers. Because of large lateral thickness variations over short distances, the selected spatial sampling (every 10 m) is probably too large to identify continuous variations of the correct frequency. To overcome this problem, a denser sampling scheme may improve the interpretation. As the low-frequency (2-3 Hz) mainly appears on the flanks of the mudslide, it may be related to a deeper interface linked to the presence of a former coarse mudslide. Other points (11 on profile B, for example) exhibited amplification at low frequencies, probably due to acquisition problems such as soil/seismometer coupling effects or local subsurface heterogeneities, which disturbed surface-wave propagation. Profile C1 is a mix between profiles CA and B. The observed frequency variations are smoother (fig. 5b), and the calculated thickness appear consistent with the geotechnical data except in the eastern part of the profile (from points 1 to 5, points 1 to 3 being located outside of the mudslide). In this area, the discrepancy between our results and geotechnical tests must come from the presence of a former coarse mudslide. Finally, the seismic noise measurements recorded for the network experiment (fig. 5d) exhibit frequencies consistent with those derived from the H/V profiles, underlying a smooth geometry of the sliding surface in this part of the mudslide.

Figure 6 presents the interpretation of the picked frequencies in term of thickness (grey points). The thickness was computed using the formula $Hs = Vs/4f_0$ with a constant shear velocity $Vs = 260$ m.s^{-1} in the mudslide. This velocity was obtained from surface wave interpretation and seismic noise network analyses (fig. 7; fig. 8). The bedrock geometry was derived from geotechnical data (black dots), photogrammetric stereo-restitution of the topography before and after the mudslide [Weber and Herrman, 2000] and H/V interpretation. The surface topography changes between 1996 (when the geotechnical tests were performed) and 2005 (when the geophysical acquisition was carried out) were taken into account. Finally, the blue dashed line corresponds
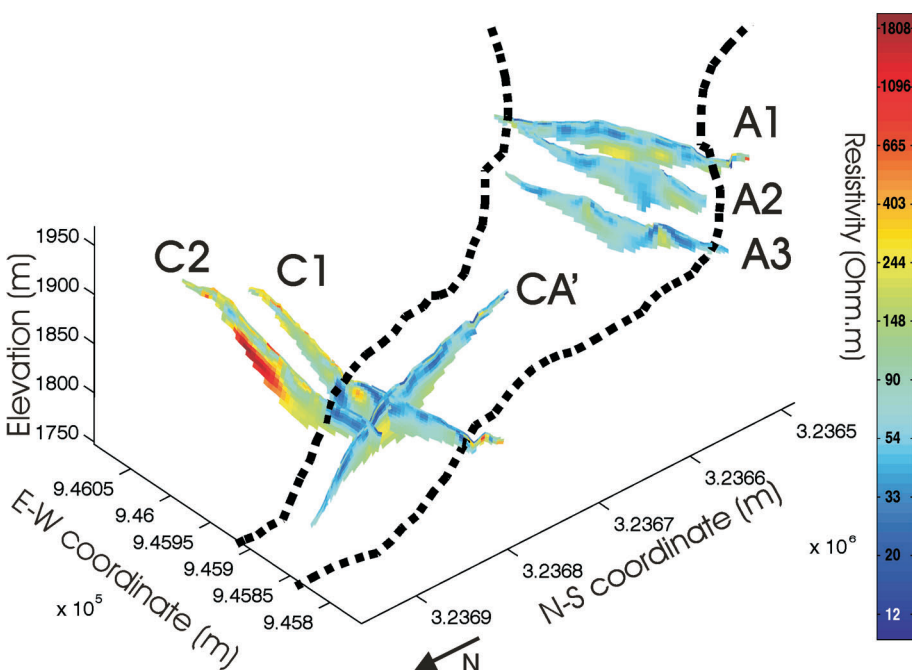

FIG. 3. – Electrical tomography images derived after inversion of data acquired using a Wenner acquisition at the "Super-Sauze" mudslide.
FIG. 3. – *Image de tomographies électriques déduites après inversion de données acquises en mode Wenner sur le glissement-coulée de "Super-Sauze".*

to the interpretation of electrical tomography sections (fig. 3). The slip surface was adjusted using geotechnical measurements. These results show that the interpretation of the picked frequency in term of thickness is particularly consistent with other measurements, even if the structure is 3D. However, it is clear that when H/V spectral ratios exhibit more than one peak in the interesting frequency range, interpretation could be ambiguous and a dense spatial sampling is needed. Variability of the mudslide shear-wave velocity can also explain the small differences between the geotechnical results and the thicknesses derived from the seismic noise data. Electrical results are consistent with the H/V data along profile CA, but less with profile C. This difference results from the lack of accuracy of the electrical tomography (smoothing effect), in particular when carried out with the Wenner configuration.

Seismic noise network

Seismic noise experiment using an array was carried out in the middle part of cross-section C (fig. 2). The array consists of three circles (radius of 10, 25 and 50 m) each composed of 6 seismic stations. To validate the dispersion curves derived from these measurements, a longitudinal active seismic profile was also recorded along profile CA (fig. 2) using 24 4.5 Hz-vertical geophones placed every 10 m apart.

Figure 7 displays the dispersion curves, the derived (S)-wave velocity models, with associated errors for the passive (fig. 7c and d) and active (fig. 7a and b) and the energy map of the surface waves. Only two seismic noise arrays (radius of 10 and 25 m) were used (transition frequency around 7 Hz on the dispersion curve), the larger one (50 m radius) presenting no dispersion effect (probably due to 3D effects for wavelengths ranging from 16 to 38 m). The two dispersion curves are consistent and display the same variations except at low frequencies (fig. 7e). This

corroborates that the seismic noise is mainly composed of surface waves, which is one of the major assumptions for 1D seismic noise interpretation.

During the inversion of the dispersion curves derived from seismic noise processing, the H/V peak frequency was added as *a priori* information. All models, which did not satisfy the resonance frequency at the central station of the array were rejected. For both the surface-wave profile and the seismic noise data, models with the lowest misfit values show (S)-waves velocity ranging between 260 and 300 m.s^{-1} in the topmost layer, with a well-defined thickness between 19-22 m for the noise data. For the surface wave profiles, the thickness is not well constrained between 14 and 24 m. These results are consistent with electrical measurements and H/V data. Within the mudslide, both inversion results showed weak Vs contrasts, which could be related to the observed superimposed units discussed before. On the contrary, the shear-wave velocity in the bedrock is not well constrained. It varies from 600 to 700 m.s^{-1} for the surface wave profiles and from 1100 to 1300 m.s^{-1} for the seismic noise data. Because of the large uncertainty on the dispersion curves of the seismic noise data at low frequencies, we only retained the velocity derived from the surface wave profile.

INVESTIGATION OF THE "SAINT-GUILLAUME" LANDSLIDE

Geological, geomorphological and geotechnical setting of the translational landslide

The "Saint-Guillaume" landslide is located in the Trièves Plateau (fig. 1) where many clayey landslides occurred in the past in the so-called varved clays; these clays are finely laminated glacio-lacustrine deposits dating from the Pleistocene
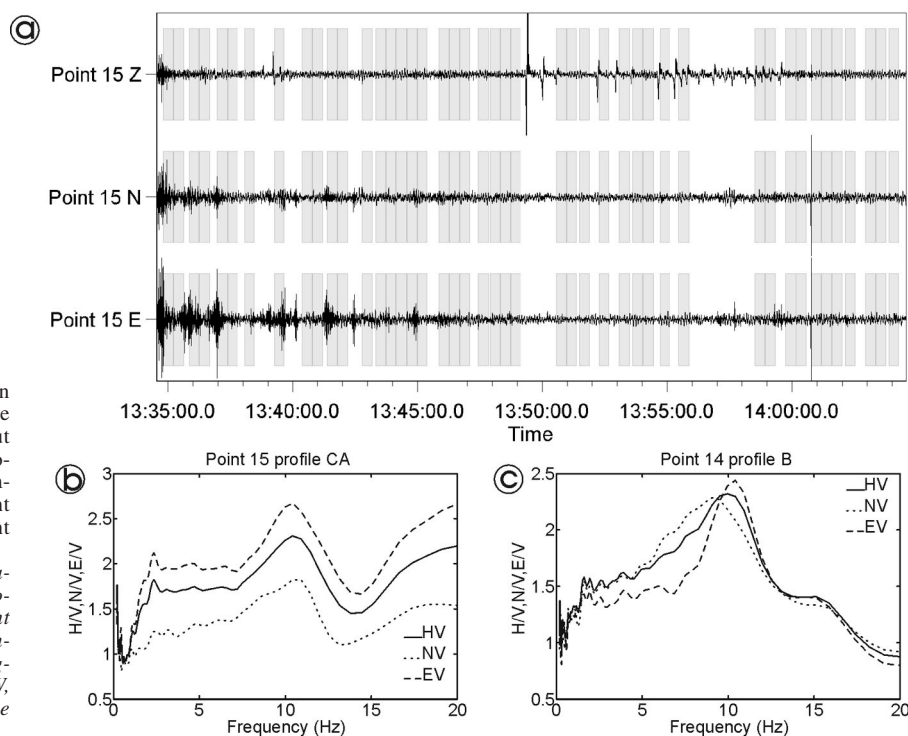

FIG. 4. – Ambient vibration data: a) ambient vibration data sampled at 200 Hz and recorded for 30 min. The grey shade indicates the short time-windows (about 40 s. in duration) selected with an anti-trigger process; b) spectral ratio computed using the E-W component, the N-S component and the H component (square root of E-W and N-S components) for point 15 of profile CA; c) for point 14 of profile B.

FIG. 4. – *Mesures de bruit de fond sismique : a) mesures de bruit de fond sismique dans le domaine temporel, échantillonné à 200 Hz et enregistré pendant 30 minutes. Le grisé indique les courtes fenêtres temporelles sélectionnées avec un processus d'anti-trigger ; b) rapports spectraux des composantes E-W, N-S et H pour le point 15 du profil CA ; c) pour le point 14 du profil B.*

(Wurmian) period [Antoine *et al.*, 1981; van Asch *et al.*, 1996]. The observed landslides present slip surfaces at different depths [Antoine *et al.*, 1981; Nieuvenhuis, 1991] from shallow ones (4 to 8 m) to more deeper ones (20 to 40 m).

The investigated landslide is a slow (1-5 cm.year^{-1}) translational landslide affecting the small village of "Saint-Guillaume". The geological basement is composed of Oxfordian marly limestone covered with 40 to 60 m of varved clays. The landslide is limited to the south by a limestone cliff overhanging a scree hillslope (fig. 8). A umbilical zone of limestone is also visible to the east sub-dividing the clay formation into two parts. To the north, the landslide is limited by the Gresse torrent, which incised a narrow channel in the varved clays. In the western part of the landslide, a geomorphological survey (geomorphological map, topographic control points) and a geotechnical investigation (with three inclinometers and one piezometer) were carried out from the late nineties [Guéguen *et al.*, 2004; Cravoisier *et al.*, 2004]. The results from the boreholes indicated the existence of an interface between the uppermost varved clay and the marly limestone bedrock at depths of 38.5 m, 61.7 m and 33.1 m for boreholes I1, I3 and I4 respectively (fig. 8). The inclinometers detected several slip surfaces inside the clay formation, with the main one and deeper located at 34.5 m, 37.0 m, and 27.0 m depth, respectively. This monitoring system has been complemented since 2003 by geophysical investigations. As a consequence, only a sum up of the main characteristics of the landslide is developed hereafter. Similarly to the "Super-Sauze" mudslide, seismic noise measurements (H/V and seismic noise network) were tested (fig. 8). The comparison with the "Super-Sauze" results is interesting because the "Saint-Guillaume" situation presents a smoother bedrock geometry and weaker (S)-wave contrasts.

H/V method

The H/V profile was carried out along an east-west direction perpendicular to the main displacement direction of the landslide (fig. 8). Measurements were made every 20 m, all along the profile, including in the village and on the marly
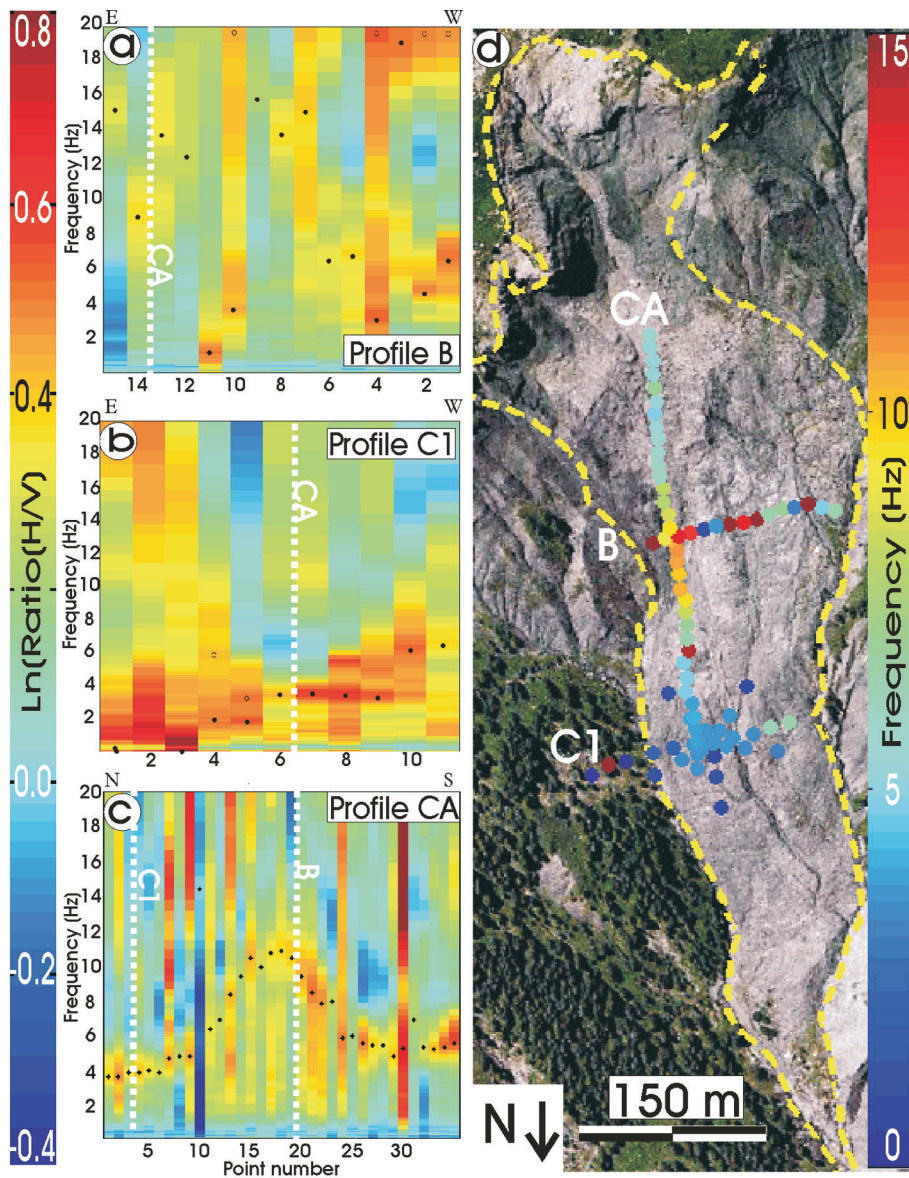

FIG. 5. – Ratio of the vertical and horizontal component (H/V) of seismic noise analysis and seismic noise network results obtained at the "Super-Sauze" mudslide: a) along profile B; b) along profile C1; c) along longitudinal profile CA; d) spatial representation of the picked frequency (displayed in colour).
FIG. 5. – *Résultats des mesures H/V obtenues sur le glissement-coulée de "Super-Sauze" : a) sur le profil B; b) sur le profil C1 ; c) sur le profil longitudinal CA ; d) représentation spatiale des pics de fréquence (représenté par un code de couleur).*

limestone bedrock outcropping at the surface (points 70 to 80). As no clear differences appear on the two horizontal spectra components, only the square root of E-W and N-S components (H) is plotted (fig. 9a). Two frequency peaks can be observed around 1.3 Hz (black dots on fig. 9a, denoted f_0) and ranging from 2 Hz to 12 Hz (circle and black dots on figure 9a, denoted f_1). The lower frequency f_0 vanishes from points 55 to 76 (high single frequency) and at the edges of the profiles (low single frequency). In the area where the bedrock outcrops (from point 71 to point 74), maximum values of the H/V ratio are irregular.

(S)-wave refraction [Guéguen *et al.*, 2004] and surface-wave analysis (fig. 10) showed that the (S)-wave velocity of the upper layer $V_{disturbed\ clays}$ is around 260 m.s^{-1}. We consequently used this velocity to calculate the landslide thickness from the highest peak frequency (fig. 9b). Black circles located below point 32 represent the known slip surface and bedrock depth derived from I3 inclinometer data. The interface lies between 0 m (where the bedrock reaches the surface) and 50 m deep. Below I3 the landslide bottom

deduced from H/V data fits very well with the surface rupture evinced by the inclinometer data. The lower frequency is more difficult to interpret. Because it vanishes where bedrock reaches the surface, it may correspond to the signature of the clay-marly limestone interface located at 61 m by inclinometer I3 (fig. 9b). For the frequency to depth conversion, we used a velocity profile that was derived from (S)-wave refraction analysis [Guéguen *et al.*, 2004] and surface waves analysis (fig. 10). Both showed that the undisturbed clays exhibit a velocity $V_{undisturbed\ clays}$ around 550 m.s^{-1}. Using an equivalent velocity based on equivalent time propagation ($Vs_{equivalent} = (H_{disturbed\ clays} + H_{undisturbed\ clays}) / (H_{disturbed\ clays}/V_{disturbed\ clays} + H_{undisturbed\ clays}/V_{undisturbed\ clays})$), the low frequency maximums were picked and converted to depth, in order to obtain an image of the bedrock topography. It is consistent with the bedrock depth measured at borehole I3 and fits remarkably with an electrical tomography profile that reaches the bedrock at a depth of 80 m [Guéguen *et al.*, 2004]. Collectively, these results suggest that the slip surface develops first at the clay/bedrock interface
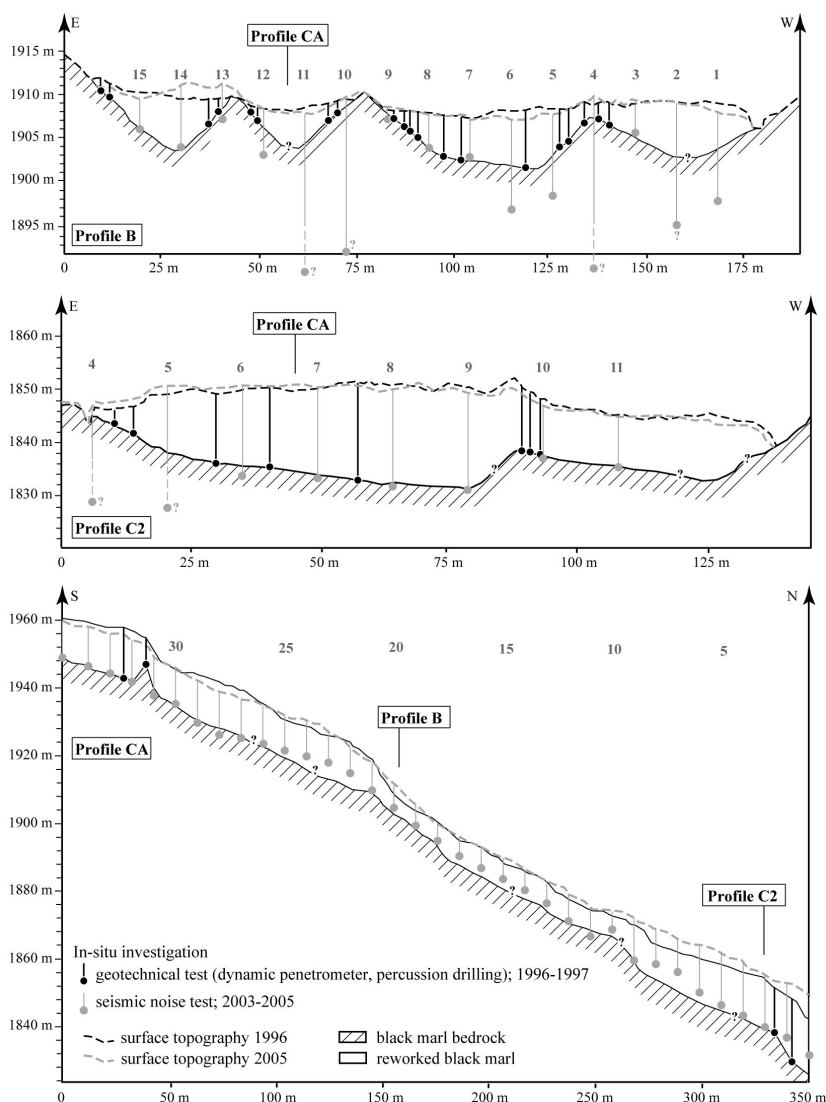

FIG. 6. – Interpretation of H/V picked frequencies on the "Super-Sauze" mudslide for the three profiles B, C1 and CA, assuming an average (S)-wave velocity of 260 m.s^{-1}. Results from geotechnical and electrical data are also shown for comparison. The interface between sliding material and stable ground was drawn considering all the results, except electrical tomography profile. The presence of two peaks in some H/V ratios (figs. 5b and 5c) resulted into two possible interpretations, although lower frequencies are expected to be due to the presence of deeper interfaces (former coarse mudslide), acquisition problems or local heterogeneity.

FIG. 6. – *Interprétation des fréquences pointées des mesures H/V sur le glissement-coulée de "Super-Sauze" considérant une vitesse de 260 m.s^{-1}. Ces interprétations sont comparées aux données géotechniques et électriques. L'interface a été dessinée considérant tous les résultats, exceptés ceux de la tomographie électrique.*

when bedrock is close to the surface and then within the clay layer (as confirmed by inclinometer monitoring). Compared to the "Super-Sauze" mudslide, the frequency picking was easier because structures are less complex and less laterally heterogeneous.

Seismic noise network

Seismic noise measurements with station arrays were carried out near the location of inclinometer I3. They involved three arrays with radius of 20, 40 and 60 m (fig. 8). Similarly to the "Super-Sauze" mudslide study, this investigation was combined with an active seismic experiment using 24 4.5 Hz-vertical geophones. The data were processed in the same way as for the "Super-Sauze" investigation. Figure 10 shows the results derived from both passive and active seismic surveys. The frequency range of the dispersion curves largely differs depending on the method. Indeed, the passive method provided useful information in the [2.5-6.5 Hz] frequency range and the active method in the [4-12 Hz] frequency range. In the [4-6.5 Hz] frequency range, the dispersion curves are remarkably similar, (fig. 10e). This observation confirms again that the largest part of the energy contained in the seismic noise is carried by surface waves. The inversion process was also performed using the H/V constraint for the passive network.

The best models (lowest RMS) for the active and passive experiments are consistent with the geotechnical and geophysical data. The (S)-wave velocity of the topmost layer is well constrained for both experiments, ranging from 260 to 280 m.s^{-1}. It corresponds to the unstable clayey zone affected by deformation, with a thickness between 31 and 34 m from the passive method and between 28 and 30 m from the active method. The difference may results from the 3D smoothing property of the array, which integrates information from a larger volume zone. Moreover, the surface wave acquisition was carried out at the N-W edge of the array.

As discussed before, (S)-wave velocities are close to 550 m.s^{-1} (Vp=1800 m.s^{-1}) in the stable clay layer and reach more than 800 m.s^{-1} (Vp 2500 m.s^{-1}) in the marly limestone bedrock. Figure 10 indicates that both methods yielded (S)-wave velocity of around 600 m.s^{-1} in the second layer (stable clay). However, they were unable to detect and characterize the bedrock top, due to the limited range of the dispersion curve at low frequency and the large data uncertainty.

CONCLUSIONS

Electrical tomography and two seismic noise experiments were carried out on two landslides with different characteristics: (1) a mudslide characterized by abrupt 3D variations

FIG. 7. – Inversion results of the dispersion curve obtained from the seismic noise network and from surface wave measurements at the "Super-Sauze" mudslide. Shear-wave velocity (Vs) models as a function of depth and of RMS error (colour scale) for a) the surface-wave data and c) the seismic noise network; b) Superimposition of the measured dispersion curve with the models derived from the surface-wave profile and d) the seismic noise array; e) superimposition of the seismic noise dispersion curve and of the semblance map of surface waves.
FIG. 7. – *Résultats de l'inversion de la courbe de dispersion du réseau de bruit de fond sismique et des mesures d'onde de surface sur le glissement-coulée de "Super-Sauze". Modèles de Vs en fonction de la profondeur et de l'erreur (échelle de couleur) pour a) les ondes de surface et pour ; c) le bruit sismique ; b) surimposition de la courbe de dispersion avec les modèles dérivés des ondes de surface et d) du bruit de fond sismique ; e) surimposition de la courbe de dispersion issue du réseau de bruit de fond sismique et de la carte de vraisemblance des ondes de surface.*
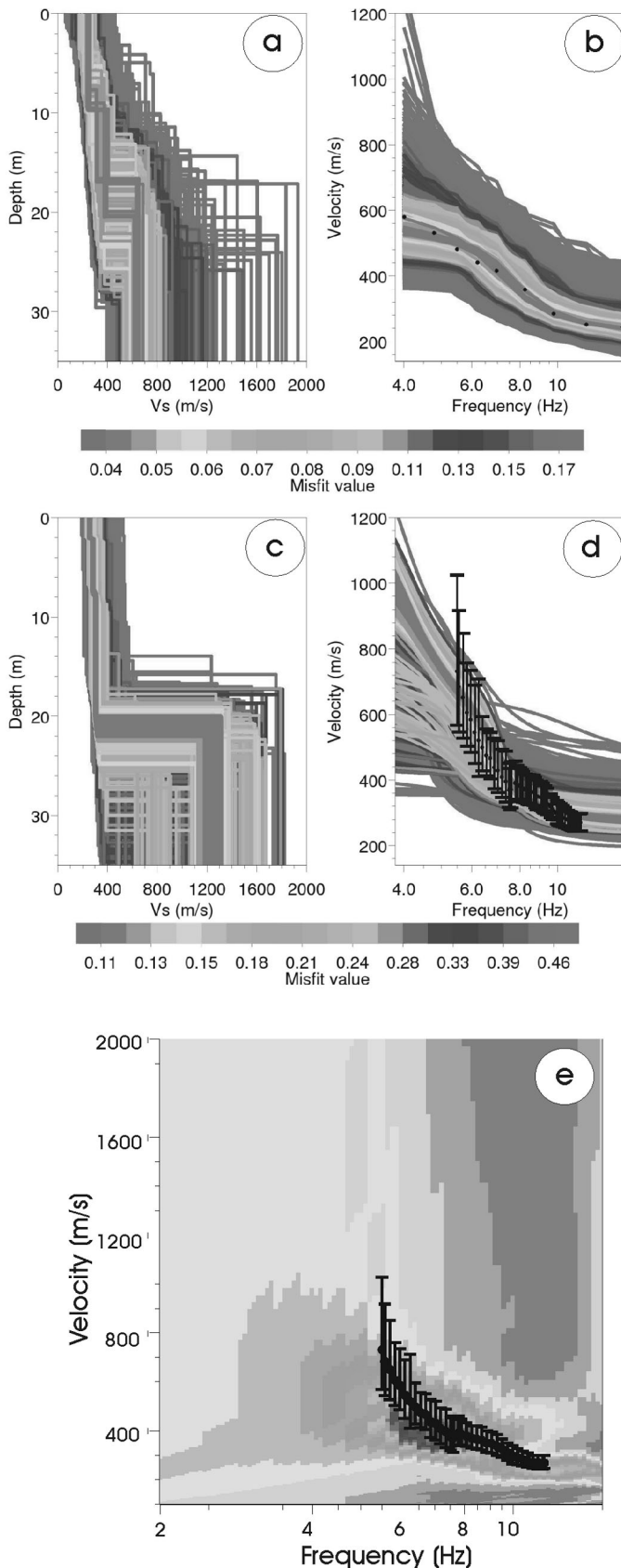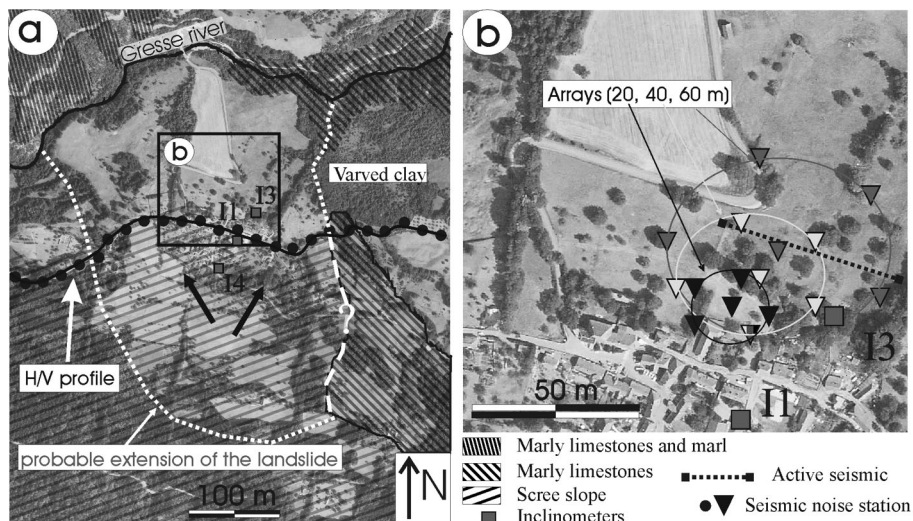
FIG. 8. – Aerial view and investigation of the
"Saint-Guillaume" landslide. a) Aerial photograph
including locations of the three inclinometers, the
locations of seismic stations and a schematic view
of the geology; b) enlargement of the zone (right)
where seismic noise investigations were carried out.
FIG. 8. – *Vue aérienne et investigation du glisse-
ment de "Saint-Guillaume". a) Photographie aé-
rienne avec la localisation des trois inclinomètres,
des mesures de bruit de fond et une vue schématique
de la géologie ; b) agrandissement de la zone d'in-
vestigation pour le réseau de bruit de fond sis-
mique.*

in the bedrock geometry and large (S)-wave con-
trasts, and (2) a translational landslide where the slip sur-
face geometry as well as the (S)-wave contrasts are
smoother. The 2D electrical tomography sections provided
valuable and continuous information about the pseudo-3D
geometry of the mudslide. H/V measurements showed their
efficiency in characterizing the contact between the stable

and unstable material in both landslides, as well as the be-
drock interface for the translational landslide. Difficulties
in H/V data interpretation arose on the mudslide, because of
multiple resonance frequencies. Some of them are perhaps
due to deeper interfaces, heterogeneities or bad coupling ef-
fects during acquisition. Our study on H/V measurements
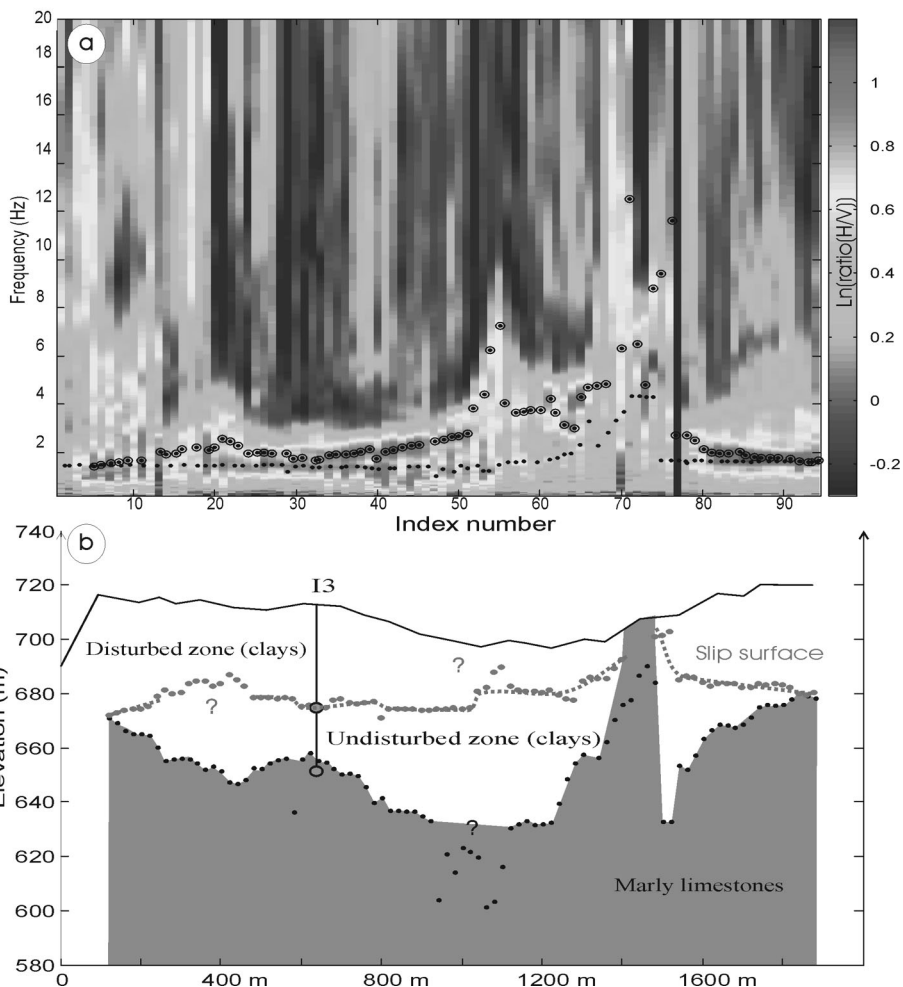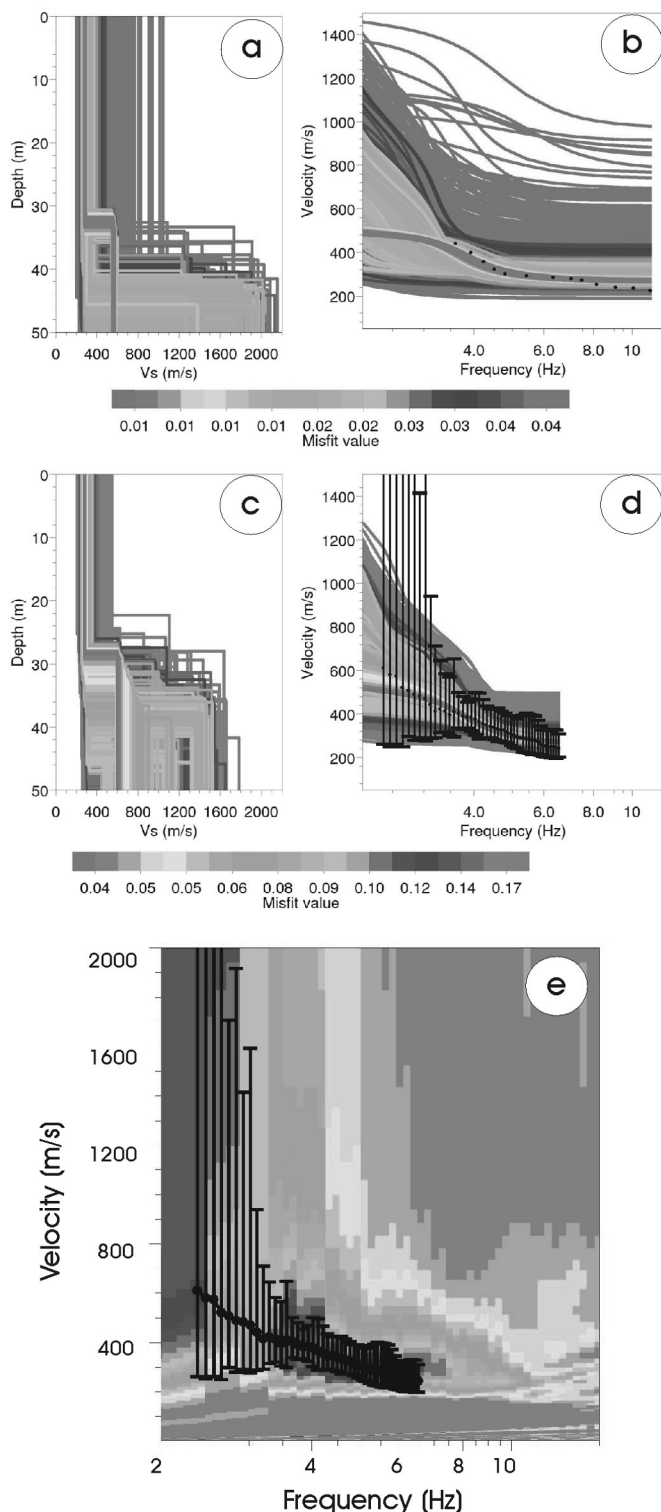on landslides demonstrates that they have to be performed

FIG. 9. – H/V measurements at "Saint-Guillaume"
landslide. a) Ratio of the vertical and horizontal
component (H/V) of seismic noise analysis measu-
red along the H/V profile (fig. 8), with the two pic-
ked frequencies (circle and black dots for higher
frequency f_1, black dots for lower frequency f_0); b)
interpretation of the picked frequencies in term of
slip surface geometry (red dots deduced from f_1)
and bedrock geometry (black dots deduced from f_0).
The grey dots represent the slip surface and bedrock
depths derived from inclinometer I3 and borehole
measurements.
FIG. 9. – *Mesures H/V obtenues sur le glissement de
"Saint-Guillaume". a) Résultats du H/V le long du
profil (fig. 8) (la basse fréquence f_0 est pointée par
les points noirs, la haute fréquence f_1 est pointée
avec les points noirs cerclés de noir) ; b) interpréta-
tion des fréquences pointées en termes de géométrie
de la surface de glissement (points rouges déduits
avec la fréquence f_1) et de géométrie du substratum
(points noirs déduits avec la fréquence f_0). Les
points gris représentent les profondeurs de la sur-
face de glissement et du substratum déduites de
l'inclinomètre I3 et des mesures en sondage.*

along profiles in order to follow frequency peaks, which can dramatically vary in heterogeneous conditions. Also the spatial sampling has to be dense enough and be adapted to the 3D geometry.

Vs profiles deduced from the seismic noise array measurements on both sites were compared to geotechnical data, as well as to results provided by active surface-wave investigations. First, the obvious similarity in the dispersion curves of the active and passive methods at the two sites indicate that the seismic noise was mainly made of surfaces waves. Secondly, we observed, particularly on the "Super-Sauze" site, that large arrays are not always efficient due to 2D/3D effects on surface waves. The largest array enabled us to record consistent dispersive waves at low frequencies on the "Saint-Guillaume" landslide.

In the two studied landslides large (S)-wave velocity contrasts were found across the slip surfaces, which were detected and measured by seismic noise methods. Consequently, combined to numerical simulations, seismic noise methods may be of high interest to identify and map slip surfaces in 3D.

FIG. 10. – Inversion results of the dispersion curve obtained from the seismic noise network and from surface wave measurements at the "Saint-Guillaume" landslide. Shear-wave velocity (Vs) models as a function of depth and of RMS error (colour scale) for a) the surface-wave data and c) the seismic noise network; b) superimposition of the measured dispersion curve with the derived models from the surface-wave profile and d) the seismic noise array; e) superimposition of the seismic noise dispersion curve and of the semblance map of surface waves.
FIG. 10. – *Résultats de l'inversion de la courbe de dispersion du réseau de bruit de fond sismique et des mesures d'onde de surface sur le glissement de "Saint-Guillaume". Modèles de Vs en fonction de la profondeur et de l'erreur (échelle de couleur) pour a) les ondes de surface et pour c) le bruit sismique ; b) surimposition de la courbe de dispersion avec les modèles dérivés des ondes de surface et d) du bruit de fond sismique ; e) surimposition de la courbe de dispersion issue du réseau de bruit de fond sismique et de la carte de vraisemblance des ondes de surface.*

References

ANTOINE P., GIRAUD A. & MONJUVENT G. (1981). – Les argiles litées du Trièves (Isère), conditions de glissement de terrain et exemples de propriétés géotechniques. – *Bull. Soc. géol. Fr.*, **XXIII**, 117-127.

ASTEN M.W. (2004). – Passive seismic methods using the microtremor wave field for engineering and earthquake site zonation. – *Proc. 74th SEG Annual Meeting*, Denver, USA, Session NGS-1.

BARD P.-Y. & BOUCHON M. (1985). – The two-dimensional resonance of sediment-filled valleys. – *Bull. Seism. Soc. Am.*, **75**, 519-541.

BONNEFOY-CLAUDET S. (2004). – Nature du bruit de fond sismique : implications pour les études des effets de site. – *Thèse de Doctorat*, Univ. J. Fourier, Grenoble, France, 241 p.

CHATELAIN J.-L., GUÉGUEN P., GUILLIER B., FRECHET J., BONDOUX F., SARRAULT J., SULPICE P. & NEUVILLE J.-M. (2000). – CityShark: A user-friendly instrument dedicated to ambient noise (microtremor) recording for site and building response studies. – *Seism. Res. Lett.*, **71**, 698-703.

COMMEND S., GEISER F. & TACHER L. (2004). – 3D numerical modelling of a landslide in Switzerland. *In: Proc. NUMOG IX*, Ottawa, Canada. – Balkema, Rotterdam, B6.

CORNOU C., KRISTEK J., OHRNBERGER M., DIGUILIO G., SCHISSELE E., GUILLIER B., BONNEFOY-CLAUDET S., WATHELET M., FAEH D., BARD P.-Y. & MOCZO P. (2004). – Simulation of seismic ambient vibrations – II: H/V and array techniques for real sites. – *In: Proc. 13th World Conf. Earth. Eng.*, Vancouver, Canada. – IAEE, Tokyo, Paper 1130, 6 p.

CRAVOISIER S., GARAMBOIS S., GUEGUEN P., MARAND A. & MONNET J. (2004). – Combined geophysical and seismological experiments on a landslide developing in varved clays. – *EGU, Geophys. Res. Abstr.*, **6**, 04065.

DAHLIN T & ZHOU B. (2004). – A numerical comparison of 2D resistivity imaging with ten electrode arrays. – *Geophys. Prospect.*, **52**, 379-398.

FIELD E. & JACOB K. (1993). – The theoretical response of sedimentary layers to ambient seismic noise. – *Geophys. Res. Lett.*, **20**, 2925-2928.

FIELD E. & JACOB K. (1995). – A comparison and test of various site-response estimation techniques including three that are not reference-site dependent. – *Bull. Seism. Soc. Am.*, **85**, 1127-1143.

FLAGEOLLET J.-C., MALET J.-P., SCHMUTZ M. & MAQUAIRE O. (2004). – Integrated investigations on landslides: example of the "Super-Sauze" earthflow. *In: Natural disaster and sustainable development*. – Springer-Verlag, Berlin, 213-238.

GALLIPOLI M., LAPENNA V., LORENZO P., MUCCIARELLI M., PERRONE A., PISCITELLI S. & SDAO F. (2000). – Comparison of geological and geophysical prospecting techniques in the study of a landslide in southern Italy. – *European J. Env. Eng. Geophys.*, **4**, 117–128.

GIRAUD A., ANTOINE P., VAN ASCH T.W.J. & NIEUWENHUIS J.D. (1991). – Geotechnical problems caused by glaciolacustrine clays in the French Alps. – *Eng. Geol.*, **31**, 185-195.

GUÉGUEN P., CHATELAIN J.-L., GUILLIER B. & YEPES H. (2000) – An indication of the soil topmost layer response in Quito (Ecuador) using H/V spectral ratio. – *Soil Dyn. and Earthquake Eng*, **19**, 127-133.

GUÉGUEN P., GARAMBOIS S., CRAVOISIER S. & JONGMANS D. (2004). – Geotechnical, geophysical and seismological methods for surface sedimentary layers analysis. *In: Proc. 13th World Conf. Earth. Eng.* Vancouver, Canada. – IAEE., Tokyo, Paper 1777, 6 p.

HASKELL N.A. (1960). – Crustal reflection of plane SH waves. – *J. Geophys. Res.*, **65**, 4147-4150.

ISRAIL M. & PACHAURI A.K. (2003). – Geophysical characterisation of landslide site in the Himalayan foothill region. – *J. Asian Earth Sc.*, **22**, 253-263.

JONGMANS D. & GARAMBOIS S. (2007). – Geophysical investigation of landslides: A review. – *Bull. Soc. géol. Fr.*, **178**. 2, 101-112.

KVAERNA T. & RINGDAHL F. (1986). – Stability of various f-k estimation techniques. – Report 1. 86/87, NORSAR Scientific Report, Kjeller, Norway, 29-40

LACHET C. & BARD P.-Y. (1994). – Numerical and theorical investigations on the possibilities and limitations of the "Nakamura's" technique. – *J. Phys. Earth (Japan)*, **44**, 377-397.

LACOSS R.T., KELLY E.J. & TOKSÖZ M. N. (1969). – Estimation of seismic noise structure using arrays. – *Geophysics*, **34**, 21-38.

LEBRUN B., HATZFELD D. & BARD P.-Y. (2001). – A site effect study in urban area: experimental results in Grenoble (France). – *Pure & App. Geophys.*, **158**, 2543-2557.

LERMO J. & CHÁVEZ-GARCÍA F. J. (1993). – Site effect evaluation using spectral ratios with only one station. – *Bull. Seism. Soc. Am.,* **83**, 1574-1594.

LOKE M.H. & BARKER R.D. (1996). – Rapid least-squares inversion of apparent resistivity pseudosections by a quasi-Newton method. – *Geophys. Prospect.*, **44**, 131-152.

MALET J.-P. (2003). – Les "glissements de type écoulement" dans les marnes noires des Alpes du Sud. Morphologie, fonctionnement et modélisation hydro-mécanique. – Thèse de Doctorat, Univ. Louis Pasteur, Strasbourg I, France, 394 p.

MALET J.-P. & MAQUAIRE O. (2003). – Black marl earthflows mobility and long-term seasonal dynamic in southeastern France. – *In: Proc.1st Int. Conf. on Fast Slope Movements*, Naples, Italy, Patron Editore, Bologna, 333-340.

MALET J.-P., VAN ASCH T.W.J., VAN BEEK L.P.H. & MAQUAIRE O. (2005). – Forecasting the behavior of complex landslides with a 2-5D spatially distributed hydrological model. – *Nat. Haz. and Earth Sys. Sc.,* **5**, 1-15.

MAQUAIRE O., FLAGEOLLET J.-C., MALET J.-P., SCHMUTZ M., WEBER D., KLOTZ S., ALBOUY Y., DESCLOÎTRES M., DIETRICH M., GUÉRIN R. & SCHOTT J.-J. (2001). – Une approche multidisciplinaire pour la connaissance d'un glissement coulée dans les marnes noires du Callovien-Oxfordien (Super-Sauze, Alpes de Haute Provence, France). – *Rev. Fr. Géotech.*, **95/96**, 15-31.

MERIC O., GARAMBOIS S., JONGMANS D., WATHELET M., CHATELAIN J.-L. & VENGEON J.-M. (2005). – Application of geophysical methods for the investigation of the large gravitational mass movement of Séchilienne, France. – *Can. Geotech. J.*, **42**, 1105-1115.

NAKAMURA Y. (1989). – A method for dynamic characteristics estimation of subsurface using microtremor on ground surface. – *Quar. Report. Railway. Tech. Res. Institute*, **30**, 25-33.

NIEUWENHUIS J.D. (1991). – The lifetime of a landslide: investigation in the French Alps. – Taylor & Francis, London, 160 p.

NOGOSHI M. & IGARASHI T. (1971). – On the amplitude characteristics of microtremor (part 2). – *J. Seism. Soc. Japan*, **24**, 26-40.

OHRNBERGER M. (2001). - Continuous automatic classication of seismic signals of volcanic origin at Mount Merapi, Java, Indonesia. – PhD Thesis, Univ. of Postdam, Potsdam, Germany, 168 p.

ROTEN D., CORNOU C., STEIMEN S., FAEH D. & GIARDINI D. (2004). – 2D resonances in Alpine valleys identified from ambient vibration wavefield. *In: Proc. 13th World Conf. Earth. Eng.,* Vancouver, Canada. – IAEE., Tokyo, Paper 1787, 6 p.

SAMBRIDGE M. (1999a). – Geophysical inversion with a neighbourhood algorithm - I. Searching a parameter space. – *Geophys. J. Int.*, **138**, 479-494.

SAMBRIDGE M. (1999b). – Geophysical inversion with a neighbourhood algorithm-II. Appraising the ensemble. – *Geophys. J. Int.*, **138**, 727-746.

SATOH T., KAWASE H. & MATSUSHIMA S. (2001). – Estimation of (S)-wave velocity structures in and around the Sendai Basin, Japan, using array records of microtremors. – *Bull. Seism. Soc. Am.*, **91**, 206-218.

SCHERBAUM F., HINZEN K.G. & OHRNBERGER M. (2003). –Determination of shallow shear wave velocity profiles in the Cologne/Germany area using ambient vibrations. – *Geophys. J. Int.*, **152**, 597-612.

SCHMUTZ M., ALBOUY Y., GUÉRIN R., MAQUAIRE O., VASSAL J., SCHOTT J.-J. & DESCLOÎTRES M. (2000). – Joint electrical and time domain electromagnetism (TDEM) data inversion applied to the Super Sauze earthflow (France). – *Surv. Geophys.*, **21**, 371-390.

STEIMEN S., FÄH D., KIND F., SCHMID C. & GIARDINI D. (2003). – Identifying 2-D resonance in microtremor wave fields. – *Bull. Seism. Soc. Am.*, **93**, 583-599.

TACHER L., BONNARD C., LALOUI L. & PARRIAUX A. (2005). – Modelling the behaviour of large landslide with respect to hydrogeological and geomechanical parameter heterogeneity. – *Landslides*, **2**, 3-14.

TOKIMATSU K. (1997). – Geotechnical site characterization using surface waves. *In:* Earthquake Geotechnical Engineering. – Balkema, Rotterdam, 1333-1368.

UEBAYASHI H. (2003). – Extrapolation of irregular subsurface structures using the horizontal-to-vertical spectral ratio of long-period microtremors. – *Bull. Seism. Soc. Am.*, **93**, 570-582.

VAN ASCH T.W.J., HENDRICKS M., HESSEL R. & RAPPANGE F.E. (1996). – Hydrological triggering conditions of landslides in varved clays in the French Alps. – *Eng. Geol.*, **42**, 239-251.

VAN ASCH T.W.J., MALET J.P., VAN BEEK L.P.H. & AMITRANO D. – Techniques, issues and advances in numerical modelling of landslide hazard. – *Bull. Soc. géol. Fr.*, **178**, 2, 65-88.

WATHELET M., JONGMANS D. & OHRNBERGER M. (2004). – Surface wave inversion using a direct search algorithm and its application to ambient vibration measurements. – *Near Surf. Geophys.*, **2**, 221-231.

WEBER D. & HERRMANN A. (2000). – Contribution de la photogrammétrie numérique à l'étude spatio-temporelle de versants instables: l'exemple du glissement de terrain de Super-Sauze (Alpes-de-Haute-Provence, France). – *Bull. Soc. géol. Fr.*, **171**, 6, 637-648.